

Superatomic Chemistry

Puru Jena

Physics Department, Virginia Commonwealth University, Richmond, VA 23284, USA

Abstract

Superatoms are atomic clusters with tailored size and composition that mimic the chemistry of atoms in the periodic table. However, unlike the atoms whose chemistry is governed by their valence electron orbitals, the chemistry of superatoms is governed by their highest occupied molecular orbitals. In addition, due to their large size and non-spherical geometry, superatoms can promote unusual reactions and serve as the building blocks of cluster assembled materials with properties very different from conventional materials. This perspective highlights the unique role of superatoms in chemical and material sciences by focusing on superhalogens, which not only possess electron affinities larger than those of halogens but also can be stable when multiply charged. We discuss how these unique features of superhalogens enable noble gas atoms like argon to form chemical bonds at room temperature and zinc to exhibit an oxidation state of +3. The advantages of using superhalogens in the synthesis of water-resistant materials for solar cells, halogen-free electrolytes for solid-state batteries, and multiferroic materials are also discussed.

1. Introduction

One of the most important contributions of chemistry to science and to mankind, for that matter, is the periodic table of elements. Developed by Mendeleev in 1869, it contains 118 elements, of which 94 occur in nature. Although the periodic table is the source of all materials, it has limitations; not only is the number of naturally occurring elements fixed, but also some of these are scarce and expensive. Equally important, the chemistry of the atoms is governed by the valence electrons and the orbitals they occupy which cannot be easily altered. For example, the noble gas atoms are chemically inert because their outer *s* and *p* electron orbitals are full, making it difficult for them to donate, accept, or share an electron. The halogens atoms, on the other hand, lack one electron to achieve shell closure, making them readily accept an electron. They have large electron affinities and are chemically reactive. Alchemists have tried for ages to manipulate the chemistry of elements, without much success.

In a seminal lecture entitled “There is plenty of room at the bottom” at the American Physical Society in 1959, Richard Feynman suggested that the properties of matter can change dramatically when reduced to nanometer length scale. Harnessing these properties, he argued, can usher a new era in materials science when nanomaterials can be synthesized and their potential for technological innovations explored. Considerable research over the past 30 years has not only revealed new phenomena in fundamental science at the nanoscale but also have validated Feynman’s vision for new technology.

Atomic clusters with varying size and composition are the ultimate nanoparticles where every atom and every electron count. Much of the current understanding of the structure and

properties of atomic clusters has emerged over the past 50 years, due to the development of new synthesis and characterization techniques as well as improved theoretical and computational methods. Atomic clusters bridge our understanding between atoms, molecules, and bulk materials, making it possible to study the evolution of their structure and properties at the atomic scale. Given that the properties of clusters are size and composition specific and very different from their bulk, they can also be used as the building blocks of a new class of materials, called cluster-assembled materials.

In this perspective, we discuss a class of atomic clusters called superatoms^{1,2}, which mimic the chemistry of atoms in the periodic table, but have properties superior to those of atoms (see Table 1). Here, emphasis is placed on superhalogens³ that not only mimic the chemistry of halogens but also can remain stable when multiply charged, promoting reactions otherwise impossible using atoms. Also discussed is the role these superhalogens play in the design and synthesis of materials for energy harvesting and storage as well as multiferroic materials. The objective is to demonstrate that understanding superatomic chemistry can enable us to produce materials with unprecedented properties.⁴

Table 1: Difference between atoms and superatoms

Atoms	Superatoms
Number of atoms is fixed	Number of superatoms is unlimited
Small size	Large size that can be varied
Spherical shape	Aspherical shape
Chemistry is governed by atomic orbitals and is fixed	Chemistry is governed by molecular orbitals and can be tailored by changing size and composition

Unstable when multiply charged	With suitable choice of size and composition can be stable when multiply charged
--------------------------------	----------------------------------------------------------------------------------

In section 2, we provide a brief introduction to superhalogens and their design, structure, and properties. The role of superhalogens in promoting unusual reactions such as enabling argon to form chemical bonds at room temperature and zinc to assume a +3-oxidation state is presented in Section 3. In Section 4, the use of superhalogens as building blocks of moisture-resistant hybrid perovskite solar cells, halogen-free electrolytes in Li-ion batteries, and multiferroic materials are discussed. Section 5 provides a summary of our conclusions and future outlook.

2. Superatoms and Superhalogens

Two of the early experiments that led to the concept of superatoms are due to Knight⁵, Castleman⁶, and coworkers. Knight et al. observed that Na clusters containing 2, 8, 20, 40, --- atoms have conspicuous peaks in the mass spectra. Assuming that Na clusters are free electron-like as is their bulk, the authors used a spherical jellium model to characterize their electronic structure and showed that the enhanced stability of clusters containing 2, 8, 20, 40, --- Na atoms is due to electronic shell closure $1S^2, 1S^2 1P^6, 1S^2 1P^6 1D^{10} 2S^2, 1S^2 1P^6 1D^{10} 2S^2 1F^{14} 2P^6 \dots$ Castleman and coworkers⁶ subsequently observed that Al_{13}^- cluster is chemically unreactive towards oxygen. Knowing that Al is trivalent and bulk Al is a free electron-like metal, the authors explained the chemistry of Al_{13}^- , which has 40 electrons, to be due to electron shell closure. Consequently, the neutral Al_{13} cluster, which has 39 electrons, should behave like a halogen atom as it too needs one extra electron for shell closure. Even though clusters do not have spherical geometry, calculations based on density functional theory with B3LYP hybrid

functional for exchange-correlation potential and Def-2tzvp basis set shows that the molecular orbitals have the same symmetry as given by the simple jellium model (see Fig. 1).

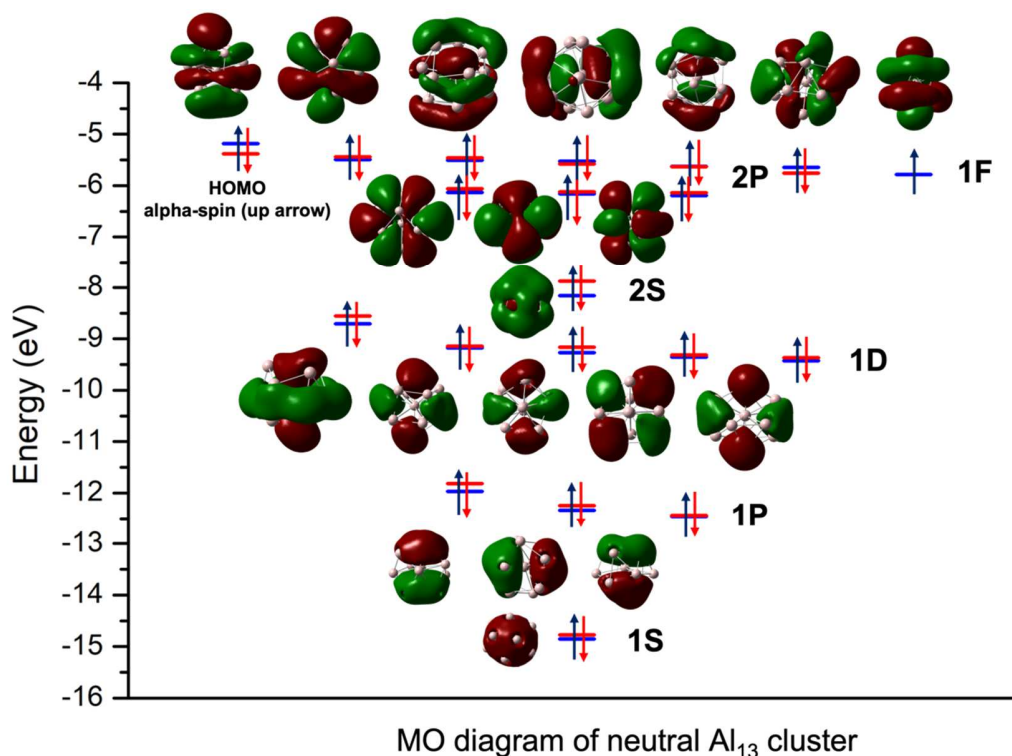


Figure 1: Frontier occupied molecular orbital diagram of neutral Al₁₃ cluster. The blue and red lines represent the energy levels corresponding to spin up and spin down electrons, respectively. The light pink sphere represents the Al atoms. Red and green regions are the electron density clouds forming 1S, 1P, 1D, 2S, 2P, and 1F shells.

The electron affinity of Al₁₃ was later found to be 3.6 eV^{7,8}, which is very close to that of the Cl atom. That Al₁₃ has the same chemistry as that of Cl was further revealed when Bowen and coworkers⁹ showed KAl₁₃ to be a salt-like molecule. Accordingly, the Al₁₃ cluster can be viewed as a superatom mimicking the chemistry of halogens. Numerous papers dealing with superatoms and their chemistry have since been published. We refer the readers to a recent

review article ⁴ by Jena and Sun for details. In the following, we focus only on one class of superatoms called superhalogens.

In fact, the word “superhalogen” was coined by Gutsev and Boldyrev³ much earlier, in 1981. According to these authors, superhalogens have the formula MX_{k+1} , where M is a metal atom of valence k , surrounded by $k+1$ halogen atoms, X. The authors showed that the electron affinity (i.e., the energy gained when an extra electron is added) of the superhalogen cluster is larger than that of a halogen atom. This is because the added electron gets distributed over $k+1$ halogen atoms, reducing electron-electron repulsion. The first experimental confirmation of superhalogens was due to Wang and coworkers¹⁰. Much of the early work on superhalogens focused on non-transition metal atoms with low atomic numbers and was guided by the octet rule. Theoretical prediction and experimental confirmation that a transition metal-based cluster, MnO_4 is a superhalogen was made by Gutsev et al.¹¹ Li et al. and Pyykko and Runenberg^{12,13} later showed that all-metal superhalogens can also be designed using the 18-electron rule. Subsequent works done in Jena’s group expanded the scope of superhalogens by using Huckel’s rule for aromatic systems¹⁴ and Wade-Mingos rule for borane-based systems.¹⁵ Superhalogens can now be designed and synthesized without using a single metal atom and/or a single halogen atom. Superhalogens that defy electron counting rules have also been suggested¹⁶. In addition, the electron affinity of clusters can be further increased by using superhalogens, instead of halogen atoms, as building blocks. These are referred to as hyperhalogens¹⁷. In the following, we discuss some of the unusual chemistry of superhalogens and the materials they can produce.

2.1 Stable Multi-anion Clusters

Most atoms in the periodic table can take an extra electron, with chlorine having the largest electron affinity of any element in the periodic table. However, no atom can retain two

extra electrons due to the strong electron-electron repulsion; the second added electron is ejected spontaneously. On the contrary, a cluster can retain two or more extra electrons if it is large or it has a unique composition. Such clusters are useful as they can promote unusual reactions, which will be demonstrated in the following. A particular cluster of interest here is icosahedral dodecaborate anion, $B_{12}H_{12}^{2-}$. With a diameter of 3.91 Å, $B_{12}H_{12}^{2-}$ is a stable dianion with the first and second electron bound by 4.56 eV and 0.9 eV, respectively. This extraordinary stability was explained by Wade and Mingos¹⁸⁻²¹ in terms of the polyhedral skeletal electron pair theory (PSEPT) that requires $n+1$ pairs of electrons where n is the number of vertices in the icosahedron. Thus, with $n=12$, $B_{12}H_{12}$ requires $(12+1) \times 2 = 26$ electrons. Note that a BH pair has 4 electrons, two of which are involved in each B-H bond. Thus, there are 24 electrons available for cage binding, but 26 are needed for stability, according to the above rule. Hence, $B_{12}H_{12}^{2-}$ is stable as a dianion. Zhao et al.²² hypothesized that the stability of $B_{12}H_{12}^{2-}$ could be further increased by replacing H by CN, thus, satisfying multiple electron-counting rules, simultaneously. The geometry of $B_{12}(CN)_{12}^{2-}$ remains icosahedral (see Fig. 2). Note that CN is a pseudo-halogen that needs an extra electron for octet shell closure and has an electron affinity of 3.82 eV. Indeed, the calculated electron affinities²² of the first and second electron of $B_{12}(CN)_{12}^{2-}$ are found to be 8.62 eV and 5.33 eV, respectively. Recently, the extraordinary stability of $B_{12}(CN)_{12}^{2-}$ has been confirmed experimentally²³ and the measured second electron affinity of 5.55 eV agrees well with the predicted value, making $B_{12}(CN)_{12}^{2-}$ the most stable dianion observed in nature. Subsequent works by Jena and his group²⁴⁻²⁷ have shown that clusters can be designed to hold up to 4 extra electrons without fragmentation or spontaneous electron emission. For example, the first, second, third, and fourth electron affinities of

$\text{BeB}_{23}(\text{CN})_{23}^{4-}$ are 9.10 eV, 6.32 eV, 4.08 eV, and 0.94 eV, respectively. In the following, we discuss the unusual chemistry such stable multi-anion complexes can promote.

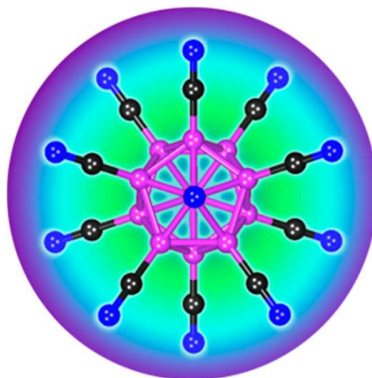


Figure 2 The geometry of $\text{B}_{12}(\text{CN})_{12}^{2-}$. Adapted with permission from ref 4.

3. Superhalogens promoting unusual reactions

In the following, we give two examples of superatoms that enable reactions otherwise impossible with atoms; multiply charged negative ion clusters binding noble gas atom argon at room temperature and Zn having an oxidation state of +3.

3.1 *Binding Ar at room temperature*

Noble gas atoms, due to their closed $s^2 p^6$ orbitals, possess high ionization potentials and vanishing electron affinities. Consequently, these electrons do not participate in chemical reactions, and noble gas atoms are chemically inert. Nearly a century ago, Pauling²⁸ suggested that Xe and Kr, due to their large size, could be polarized and form stable compounds. In 1962, Bartlett²⁹ synthesized the first stable compound of $\text{Xe}^+[\text{PtF}_6]^-$. Several compounds of Xe and Kr have since been synthesized³⁰⁻³². But, making argon to form a stable compound at room temperature remained a challenge. HArF^{33} is the only neutral Ar-containing compound that has

been isolated in a low-temperature matrix. Here, the Ar atom forms an “insertion compound” where the HAr moiety carries a positive charge and F carries compensating negative charge. Samanta³⁴ showed that the binding of Ar, as well as charge transfer to HAr, can be enhanced if F is replaced by a superhalogen, Y, such as BO₂ and BF₄. However, the binding energy is still small and Ar forming a stable compound with at room temperature remained a desired goal.

Recently, Mayer et al.²³ studied the interaction of Ar with B₁₂(CN)₁₁⁻ cluster. Recall that B₁₂(CN)₁₂ can gain 13.95 eV energy by accepting two electrons while the electron affinity of PtF₆ is only 8.0 eV. Secondly, once a CN moiety is removed from B₁₂(CN)₁₂²⁻, the B atom on the icosahedral cage remains positively charged while the entire B₁₂(CN)₁₁⁻ cluster carries a negative charge. Thus, B₁₂(CN)₁₁⁻ is a unique cluster where a positive charge on B and a negative charge on the entire cluster cage (see Fig. 3) creates an electric field capable of polarizing an Ar atom. Indeed, Mayer et al. showed that Ar is bound to B₁₂(CN)₁₁⁻ at room temperature with a binding energy of 0.63 eV. Zhou et al. have shown that the binding of Ar can not only be further enhanced by removing a second CN⁻ moiety from B₁₂(CN)₁₁⁻ but also B₁₂(CN)₁₀ can bind two Ar atoms.

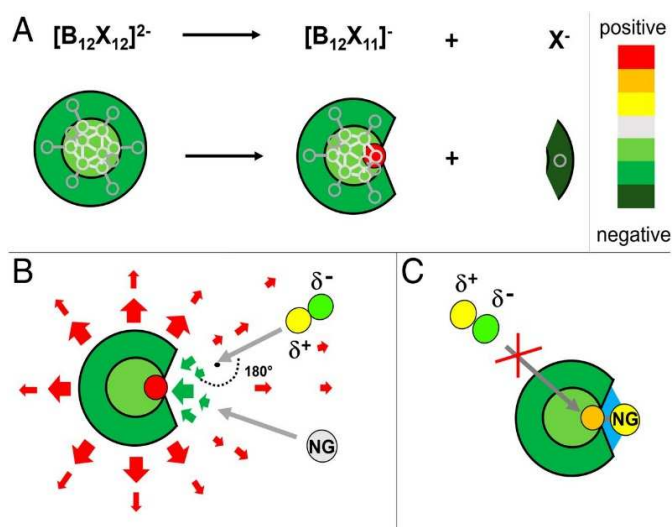


Fig.3 (A) Schematic representation of the interaction of a noble gas atom with electrophilic anion $[B_{12}X_{11}]^-$. Adapted with permission from ref 23.

3.2 Zn in +3 oxidation state

The oxidation state of an element is the number of electrons it can lose in a chemical reaction. While elements with low atomic numbers have a single oxidation state, transition metal elements with unfilled *d*-shells exhibit multiple oxidation states. Consider, for example, Zn and Hg; both belong to the same Group 12 element. Yet, Zn, with an outer electron configuration of $4s^2 3d^{10}$, has an oxidation state of +2 while Hg, due to relativistic effects, exhibits oxidation states of +2, +3, and +4³⁵⁻³⁸. Attempts^{39,40} have been made to see if Zn can exhibit an oxidation state of +3 if interacted with electronegative species such as F, BO_2 , and AuF_6 , whose electron affinities are 3.4 eV, 4.5 eV, and 8.4 eV, respectively. Note that for Zn to exhibit an oxidation state of +3, it not only needs to bind to three monovalent species with significant binding energy, but also have its *3d* electrons explicitly participate in bonding. Although $Zn(AuF_6)_3$ was found to be a stable cluster, the binding energy is still very small and no direct participation of Zn's *3d* electrons was noticed. Since it takes 39.7 eV to detach three electrons from Zn, one has to find suitable super electrophilic reagents.

As pointed out above, recently, several clusters have been identified as being stable in multiply charged states²²⁻²⁷ and as much as 20 eV can be gained by adding three extra electrons. Fang et al.⁴¹ studied the interaction of Zn with super electrophilic clusters $BeB_{11}(CN)_{12}^{3-}$ and $BeB_{23}(CN)_{22}^{3-}$ whose first, second, and third electron affinities are 8.44 eV, 4.76 eV, 2.65 eV, and 8.86 eV, 6.38 eV, 3.25 eV, respectively. In addition, the total energy gained in adding the three electrons ($EA_1 + EA_2 + EA_3$) is 18.49 eV for $BeB_{23}(CN)_{22}$ and 15.85 eV for $BeB_{11}(CN)_{12}$, making these clusters extraordinary electrophiles. Geometries of these clusters are given in Fig.

4A and 4B. Corresponding geometries of Zn interacting with $\text{BeB}_{11}(\text{CN})_{12}$ and $\text{BeB}_{23}(\text{CN})_{22}$ are given in Fig. 4C and Fig. 4D, respectively.

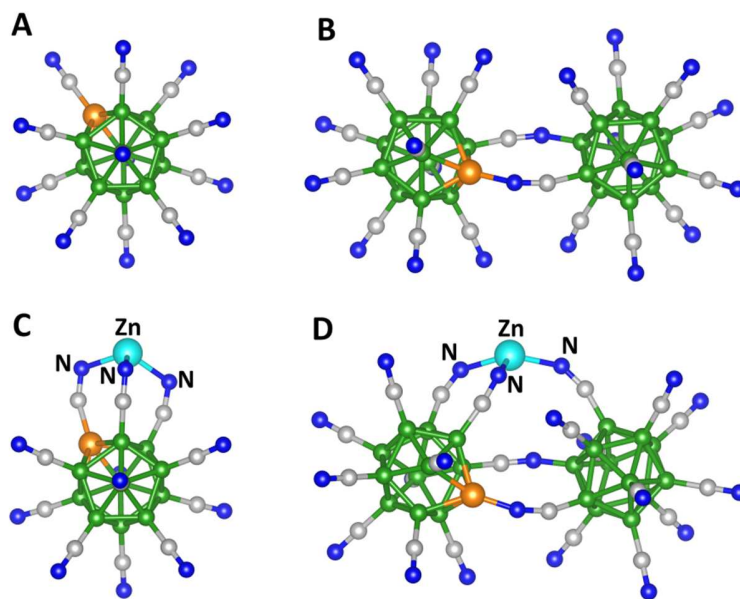


Fig. 4 Equilibrium geometries of (A) $\text{BeB}_{11}(\text{CN})_{12}^{3-}$, (B) $\text{BeB}_{23}(\text{CN})_{22}^{3-}$, (C) neutral $\text{ZnBeB}_{11}(\text{CN})_{12}$ and (D) neutral $\text{ZnBeB}_{23}(\text{CN})_{22}$. Boron, carbon, nitrogen, beryllium, and zinc atoms are in green, grey, blue, orange, and cyan, respectively. Adapted with permission from ref. 41.

Note that Zn binds to three N atoms. In addition, the Zn-N bond lengths in these clusters range between 1.94 Å to 2.01 Å and are smaller than those in the known compounds. The binding energies E_b of the ZnY [$Y = \text{BeB}_{11}(\text{CN})_{12}, \text{BeB}_{23}(\text{CN})_{22}$] complexes are calculated using the formula,

$$E_b = -[E(\text{ZnY}) - E(\text{Zn}) - E(\text{Y})].$$

Here, E is the total energy of the respective clusters. E_b 's for Zn $\text{BeB}_{11}(\text{CN})_{12}$ and Zn $\text{BeB}_{23}(\text{CN})_{22}$ are 6.33 eV and 7.04 eV, respectively. In comparison, $\text{Zn}(\text{AuF}_6)_3$ is stable⁴⁰ against

dissociation to $\text{Zn}(\text{AuF}_6)_2 + \frac{1}{2}\text{Au}_2\text{F}_{10} + \frac{1}{2}\text{F}_2$ by only +0.26 eV at the DFT/B3LYP level of theory. Note that the above binding energies of ZnY are larger than the 3.91 eV binding energy of Zn in the ZnO dimer where Zn has an oxidation state of +2. According to the natural bond orbital (NBO) charge analysis, the charges on Zn in $\text{ZnBeB}_{11}(\text{CN})_{12}$ and $\text{ZnBeB}_{23}(\text{CN})_{22}$ are 1.3 times more positive than that of Zn in the ZnO dimer. The large binding energies, as well as the large positive charge associated with Zn in these clusters, indicate that the bonding of Zn in these super electrophilic species is fundamentally different from that in the known compounds where Zn is in the +2-oxidation state.

Further evidence that Zn is in a +3-oxidation state is obtained by analyzing the partial density of states, projected crystal Hamiltonian population, electron localization function, and energy decomposition. The charge density differences, calculated by subtracting the charge densities of the Zn atom and the electrophilic clusters from the total charge density of the zinc-bonded cluster are shown in Fig. 5. In both cases, the charge densities are positive around the middle of the Zn-N bonds and negative in areas surrounding Zn and N atoms. These suggest that both ionic and covalent types of bonding are prevalent in the interaction between Zn and N.

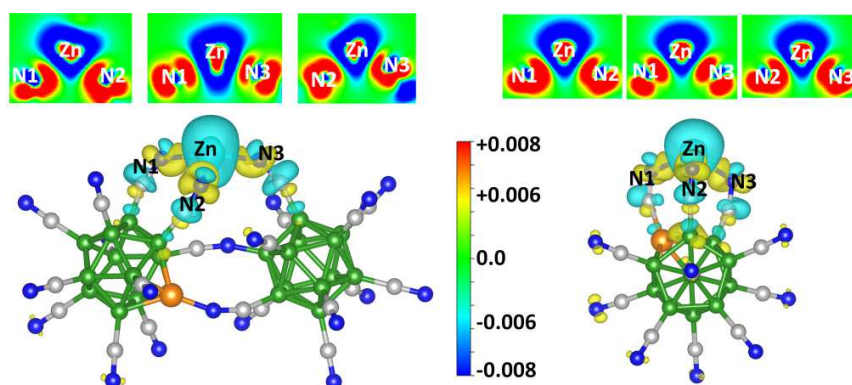


Fig. 5 Charge density difference for $\text{ZnBeB}_{23}(\text{CN})_{22}$ (**Left**) and $\text{ZnBeB}_{11}(\text{CN})_{12}$ (**Right**). The top and bottom panel shows the CDD along the N-Zn-N bond in 2D and 3D, respectively. Adapted with permission from Ref. 41.

Explicit participation of Zn(*d*) electrons with N(*p*) and N(*s*) electrons can also be seen from the partial densities of states (DoS) in Fig. 6. Further analysis of the electron localization function and energy decomposition complement the results above, i.e., Zn behaves as if it has an oxidation state of +3.

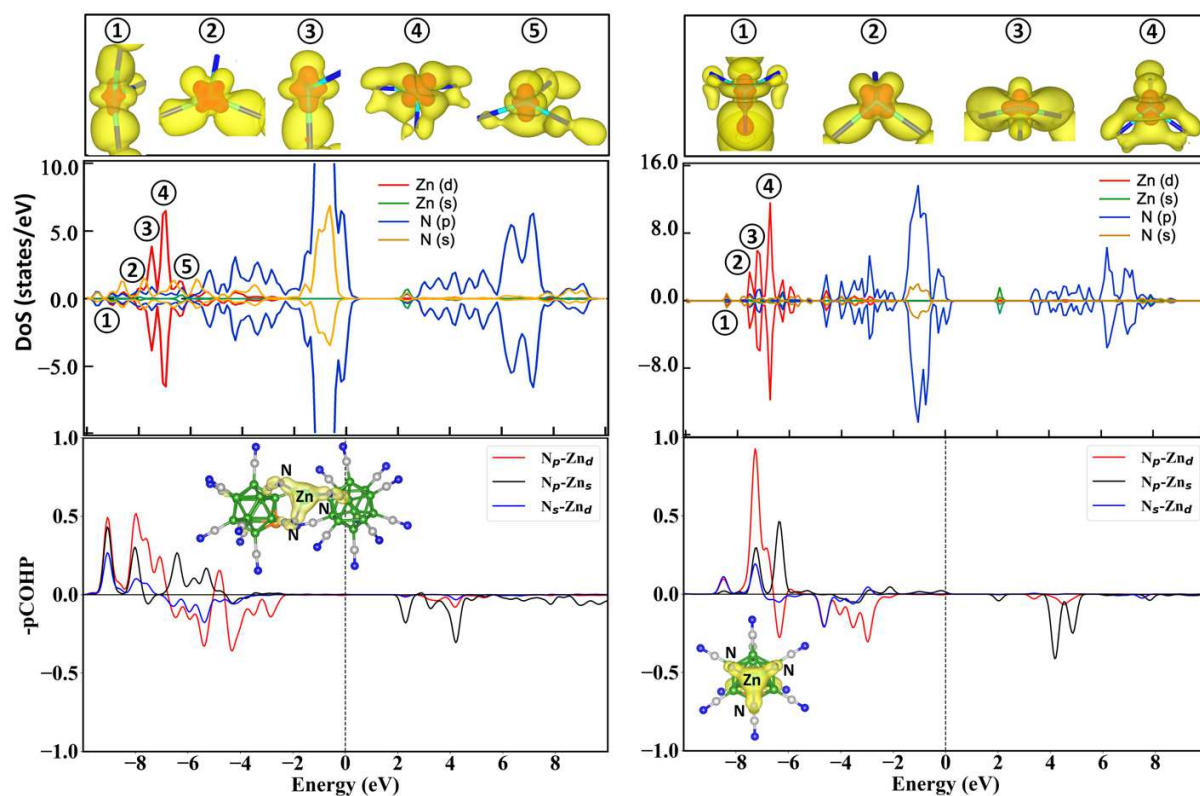


Fig. 6 (Top panel) Partial charge density for spin-up and spin-down electrons with an isovalue of $0.002 e/\text{Bohr}^3$ in yellow and $0.06 e/\text{Bohr}^3$ in red and (bottom panel) Crystal Hamiltonian population analysis for $\text{ZnBeB}_{23}(\text{CN})_{22}$ and $\text{ZnBeB}_{11}(\text{CN})_{12}$. Here, positive and negative values correspond to the bonding and antibonding state, respectively. The insets show the partial charge density of all the bonding states for the three Zn-N bonds. Adapted with permission from Ref. 41.

To show that the superatomic chemistry of $\text{BeB}_{11}(\text{CN})_{12}$ and $\text{BeB}_{23}(\text{CN})_{22}$ electrophiles is clearly different from that of atomic chemistry, we compare the above results with ZnN hetero

dimer. Note that the N atom needs three extra electrons to satisfy its octet shell closure, just as $\text{BeB}_{11}(\text{CN})_{12}$ and $\text{BeB}_{23}(\text{CN})_{22}$ need three extra electrons to satisfy the Wade-Mingos rule. In ZnN , however, Zn is an oxidation state of +2 as its $3d$ electrons do not take part in chemical bonding. Furthermore, ZnN 's binding energy of 2.31 eV is about a factor of three smaller than that in $\text{ZnBeB}_{23}(\text{CN})_{22}$ and $\text{ZnBeB}_{11}(\text{CN})_{12}$. Energy decomposition analysis of ZnN compared to that in $\text{ZnBeB}_{11}(\text{CN})_{12}$ and $\text{ZnBeB}_{23}(\text{CN})_{22}$ shows that the magnitudes of the electrostatic interaction (ΔE^{ele}) and electron exchange interaction (ΔE^{ex}) in $\text{ZnBeB}_{11}(\text{CN})_{12}$ are much greater than those in ZnN dimer, suggesting a greater extent of charge transfer from Zn to N in the former.

4. Superhalogens as building blocks of materials

Superatoms can be used as building blocks of materials whose properties can be very different from materials built from atoms with similar chemistry. This is because the superatoms have a larger size and aspherical symmetry than the atoms whose chemistry they mimic. Here, we illustrate this difference by focusing on superhalogens as building blocks of halogen-free electrolytes in Li-ion batteries, moisture-resistant hybrid perovskites for solar cells, and multiferroic materials.

4.1 Solid electrolytes for Li-ion batteries

In Table 2, we list some of the current electrolytes in Li-ion batteries. These are complex salts with Li as the cation and AsF_6 , BF_4 , PF_6 , FePO_4 , LiClO_4 , $\text{N}(\text{SO}_2\text{F})_2$, and $\text{N}(\text{SO}_2\text{CF}_3)_2$ as the anions. Because of their large size and electron affinity, these anions can be viewed as superhalogens.⁴² Most of these electrolytes contain halogen atoms that are toxic and corrosive. Hence, there is interest in developing halogen-free electrolytes. Note that BH_4 , with an electron

affinity of 4.50 eV, is a superhalogen that is halogen-free. LiBH₄ is a superionic conductor, but only at high temperature (~390 K). Noting that CB₁₁H₁₂ is a superhalogen which is larger than BH₄ and also has a larger electron affinity of 5.99 eV, Giri et al.⁴² studied the potential of LiCB₁₁H₁₂ as a halogen-free electrolyte. They suggested that for an ideal electrolyte, the energy, ΔE , to dissociate the electrolyte into a Li cation and superhalogen anion [$\Delta E = -\{E(\text{LiX}) - E(\text{Li}^+) - E(\text{X}^-)\}$], as well as its binding energy with H₂O [$E_b = -\{E(\text{LiXH}_2\text{O}) - E(\text{LiX}) - E(\text{H}_2\text{O})\}$], should be small. They computed ΔE and E_b for LiCB₁₁H₁₂ and compared these values with electrolytes used in Li-ion batteries. The results are summarized in Table 2.

Table 2. Vertical Detachment Energies (VDEs), Energies to Dissociate the Li Salt into Individual Ions (ΔE), and Binding Affinity (E_b) to H₂O of Currently Used and Predicted Electrolytes. Adapted with permission from Ref. 42.

Negative ions	VDE in eV	ΔE in eV	E_b in eV
[AsF ₆] ⁻	8.91	5.65	1.09
[BF ₄] ⁻	7.66	6.08	1.41
[PF ₆] ⁻	8.55	5.73	1.07
[FePO ₄] ⁻	4.32	7.38	1.04
[ClO ₄] ⁻	5.83	5.96	1.02
[N(SO ₂ F) ₂] ⁻	6.89	5.82	1.02
[N(SO ₂ CF ₃) ₂] ⁻	7.01	6.01	0.99
NO ₃	4.22	6.53	0.96
BH ₄	4.50	6.62	0.92
B ₃ H ₈	4.72	6.25	0.93
CB ₁₁ H ₁₂	5.99	5.08	1.08

Note that the energy to dissociate LiC₁₁H₁₂ into individual ion components is the smallest among all the electrolytes. Its affinity towards water, on the other hand, is at par with other electrolytes.

The authors suggested that $\text{LiC}_{11}\text{H}_{12}$ could be an ideal halogen-free electrolyte for Li-ion batteries. Subsequent experiments have confirmed this prediction^{43,44}.

Li-rich antiperovskites (LiRAP) with formula Li_3OX ($\text{X}=\text{halogen}$) are another class of promising solid-state electrolytes⁴⁵ for Li-ion batteries. These materials exhibit high room-temperature ionic conductivity, low activation energy, large electrochemical stability window (ESW), low electronic conductivity, and excellent electrochemical stability against lithium metal anode. In addition, they can be further functionalized by replacing halogens with superhalogens such as BH_4 and BF_4 . Due to their larger size, superhalogen-based LiRAP provides increased channel space for Li-ions to migrate, and due to their non-spherical geometry, rotational motion alters the potential energy landscape, possibly lowering the activation barrier. Both these factors enhance the ionic conductivity. Fang and Jena⁴⁶ studied the crystal structure, stability, and ionic conductivity of Li_3OY and Li_3SY ($\text{Y}=\text{BH}_4, \text{AlH}_4, \text{BF}_4$) and LiRAPs with mixed halogen and superhalogens. They showed that superhalogen-based LiRAPs can indeed exhibit enhanced ionic conductivity. The crystal structure, phonon frequencies, electron density of states radial distribution function, and ionic conductivity are shown in Fig. 7. Because of their positive phonon frequencies, these materials are lattice-dynamically stable. The formation energy of Li_3SBF_4 calculated for the reaction $\text{LiBF}_4 + \text{Li}_2\text{S} \rightarrow \text{Li}_3\text{SBF}_4$ is 39.4 meV/atom. This is significantly lower than 58.8 meV/atom for the reaction $\text{LiBH}_4 + \text{Li}_2\text{O} \rightarrow \text{Li}_3\text{OBH}_4$ and comparable to that of 25.8 meV/atom for the reaction $\text{LiBr} + \text{Li}_2\text{O} \rightarrow \text{Li}_3\text{OBr}$. In addition, the energy band gap of Li_3SBF_4 is 8.5 eV, which is larger than that of Li_3SAIH_4 (5.0 eV), Li_3OBH_4 , (7.0 eV) and Li_3OA ($\text{A} = \text{halogen}$). As the bandgap provides a measure of the electrochemical stability window, Li_3SBF_4 has the potential to be an ideal electrolyte. The melting point of

Li_3SBF_4 above 600K and its linear thermal expansion coefficient of $0.6 \times 10^{-5}/\text{K}$ add further advantages to this material. The calculated room temperature (RT) conductivity of Li_3SBF_4 , namely, 1.0×10^{-2} S/cm, is much larger than the experimentally observed RT conductivity of Li_3OCl , namely, 0.85×10^{-3} S/cm, and is comparable to that of the organic liquid electrolyte used in practical batteries. The superionic conductivity can be further increased to 1.9×10^{-2} S/cm by partially replacing BF_4^- with Cl^- . Note that Li_3S and Li_3O are superalkalis as they have one more electron than needed for shell closing. Thus, Li_3SBF_4 can be considered as a “supersalt” surpassing the properties of conventional salts.

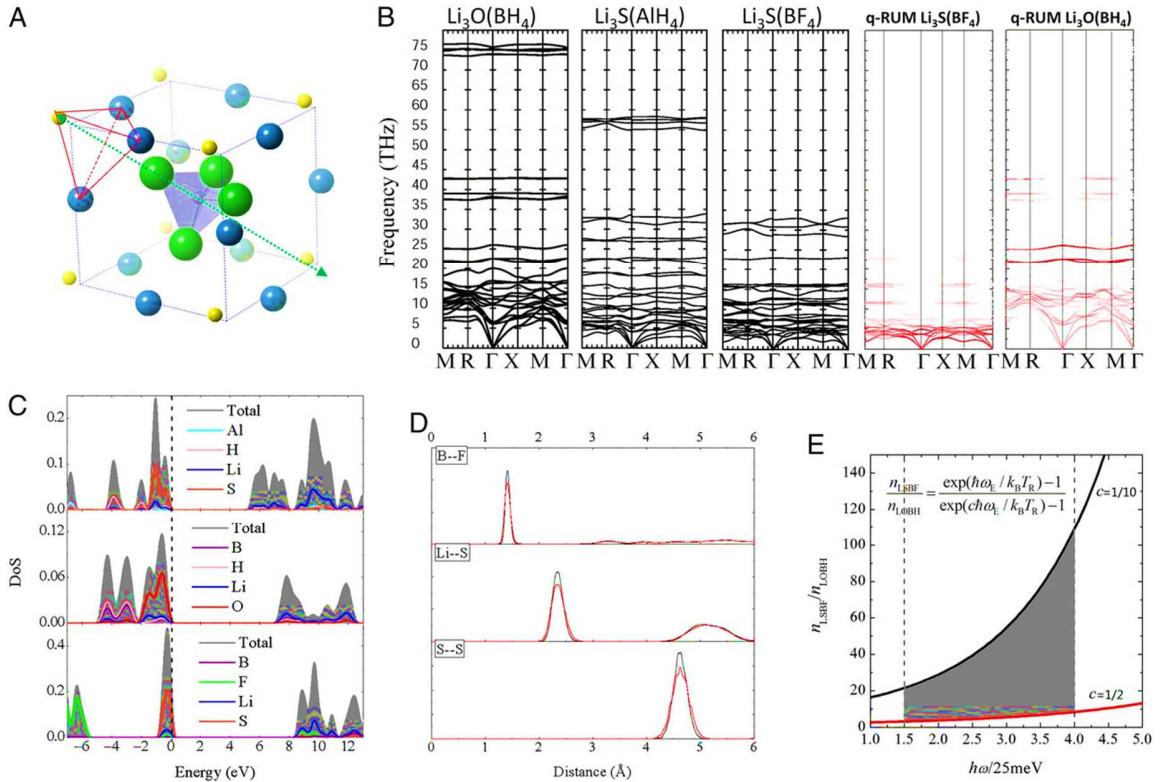


Figure 7. (A) Optimized unit cell of Li_3SBF_4 , with Li, S, B, and F in blue, yellow, gray, and green, respectively. (B) Phonon spectra of the studied super-LRAP. (C) Partial DoS. With the Fermi level set to zero. (D) Radial distribution functions of Li_3SBF_4 . (E) Estimated range of

ratio between the ionic conductivity of Li_3SBF_4 and Li_3OBH_4 at room temperature. Adapted with permission from ref 46.

4.2 Moisture-resistant hybrid perovskites solar cells

Superhalogens can also play a role in improving the material properties of organic-inorganic hybrid perovskites $\text{A}^+(\text{MX}_3)^-$ solar cells [$\text{A} = \text{CH}_3\text{NH}_3, \text{HC}(\text{NH}_2)_2$; $\text{M} = \text{Pb}, \text{Sn}, \text{Ge}$; $\text{X} = \text{Cl}, \text{Br}, \text{I}$] whose efficiency in the last 10 years has increased from about 3% to over 20%. They are easy to synthesize and have excellent light emission properties and tunable bandgaps.⁴⁷ In Fig. 8, we show the lattice structure⁴⁸ of $\text{A}^+(\text{PbI}_3)^-$. However, these materials degrade fast when exposed to intense light or moisture. To understand the sensitivity of these materials towards H_2O , Fang and Jena⁴⁹ realized that the geometry of the organic cation CH_3NH_3 in the perovskite is the same as that in the gas phase. In addition, the ionization potential of CH_3NH_3 , namely 4.13 eV, is smaller than that of an alkali atom and, hence, it can be regarded as a superalkali. Similarly, the inorganic anion, PbI_3 can also be regarded as a superhalogen and, thus, $\text{CH}_3\text{NH}_3\text{PbI}_3$ is a supersalt.

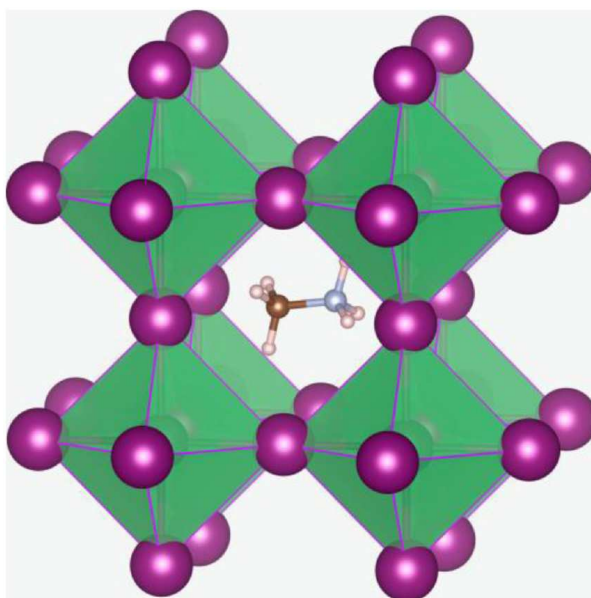


Figure 8 Crystal structure of $\text{CH}_3\text{NH}_3\text{PbX}_3$ perovskites ($X = \text{I}, \text{Br}, \text{and/or Cl}$). Adapted with permission from Ref. 48.

To understand the cause of perovskite's sensitivity to moisture and to suggest ways to alleviate this problem, the authors used a cluster model to simulate the interaction of $\text{CH}_3\text{NH}_3\text{PbI}_3$ cluster with water. In Fig. 9, we show the molecular dynamics simulation of the interaction between $\text{CH}_3\text{NH}_3\text{PbI}_3$ and H_2O . As the water molecule enters into the bond between CH_3NH_3^+ and PbI_3^- , H^+ pointing towards I^- results in the formation of HI while OH^- attracts H^+ from CH_3NH_3^+ to form H_2O and CH_3NH_2 . As HI and CH_3NH_2 are volatile, this leaves the system with PbI_2 and one less hybrid perovskite moiety. The process continues until all that is left is H_2O and PbI_2 .

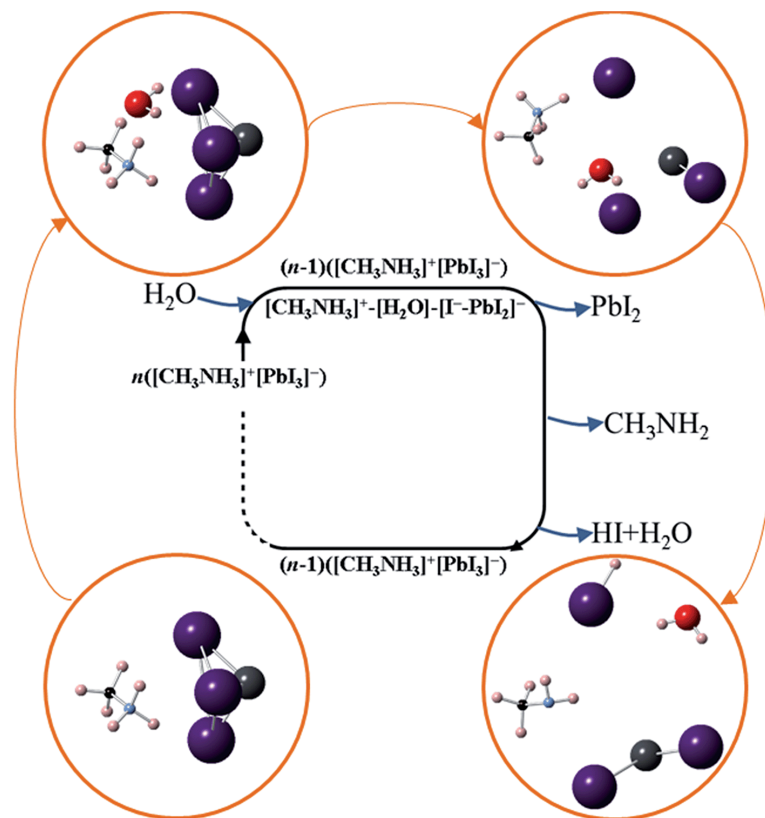


Figure 9. Degradation mechanism of $\text{CH}_3\text{NH}_3\text{PbI}_3$ exposed to moisture. The ball-and-stick plots (Pb, lead black; I, purple; N, cyan; C, black; O, red; H, pink) in the circles demonstrate the process in sequence as indicated by the arrows. Adapted with permission from Ref. 49.

To mitigate this problem, Hong and Jena replaced halogen I in PbI_3 with BH_4 superhalogen and studied the interaction of H_2O with $\text{CH}_3\text{NH}_3\text{Pb}(\text{BH}_4)_3$ cluster. Note that the size of BH_4 is similar to that of I. Thus, replacing I with BH_4 would not compromise the stability of the modified perovskite. The advantage of replacing I by BH_4 is that while I^- carries the extra electron, it is distributed over four H atoms of BH_4 , thus reducing the attraction between $\text{H}^{\delta+}$ and $\text{H}^{\delta-}$. Indeed, the hybrid perovskites consisting of hyperhalogens $[\text{Ge}/\text{Sn}(\text{BH}_4)_3]$ show significantly reduced (about 20%) binding energy with the water molecule, as compared to the materials with superhalogens $[\text{Ge}/\text{SnX}_3]$ ($X = \text{halogen}$). Note that Schouwink et al.⁵⁰ have successfully replaced halogens in perovskites with BH_4 and synthesized more than 30 new perovskite crystals.

4.3 Ferroelectric materials

Ferroelectric materials are dielectric materials in which polarization remains permanently even after the applied electric field is removed and the direction of the dipole moment can be switched by applying an electric field. Because of their many technological applications, there is a great deal of interest in finding efficient ferroelectric materials composed of earth-abundant and non-toxic elements. Perovskites such as PbTiO_3 are among the prevalent ferroelectric materials. As pointed out earlier, perovskites can be modified by replacing the cationic and anionic components by superalkali cations and/or superhalogen anions, respectively. Here, the large electron affinity of the superhalogens and low ionization energy of the superalkalis may enhance the amount of charge transfer and their large size may increase the charge transfer distance. Both factors would lead to giving rise to higher dipole moments. The aspherical

geometry may also break centro-symmetry. Thus, a combination of these factors may enable superatoms to be ideal building blocks of a new generation of ferroelectric materials with improved properties. Here, we discuss these possibilities by considering superatom-based zero-, one, two- and three-dimensional ferroelectric materials.

4.3.1 Zero-dimensional functionalized C_{60} fullerene

C_{60} fullerene⁵¹ is a well-known cluster that has been synthesized in bulk quantities and retains its structure when assembled. Composed of 12 pentagons and 20 hexagons, C_{60} is non-polar. However, C_{60} can be made into a polar molecule by functionalization with dopants, ligands, or endohedral atoms. Several $M@C_{60}$ endohedral complexes have been synthesized^{52–58}. The endohedral metal atom, M can occupy the center site or the off-center site if its radius is smaller than that of the C_{60} cluster. In the latter case, the site above the center of a hexagon is lower in energy than the site over the center of the pentagon. The polarization is switched when the M ion hops to adjacent hexagonal or pentagonal rings along the inner wall of the C_{60} cage. Wu and coworkers⁵⁹ studied the hopping from hexagon-to-hexagon and hexagon-to-pentagon and found that the barrier for the former is lower in energy compared with that of the latter. For applications, the ideal range of the switching barrier has been estimated to be approximately between 0.1 to 1 eV. This is large enough to prevent quantum tunneling while moderate enough for hexagon-to-pentagon switching.⁵⁹ The switching pathway of M from one hexagon to an adjacent one using the NEB method is shown in Fig. 10(a)⁶⁰. In $M@C_{60}$, the switching barriers are 0.02 eV, 0.40 eV, and 0.23 eV for $M=Li, Fe,$ and $Mn,$ respectively. While the barrier in $Li@C_{60}$ can be easily overcome by thermal fluctuation under ambient conditions, those for $Fe@C_{60}$ and $Mn@C_{60}$ are within the desirable range. Because Mn and Fe ions carry a magnetic moment of 3 and 2 μ_B , respectively, these metallofullerenes are multiferroic.

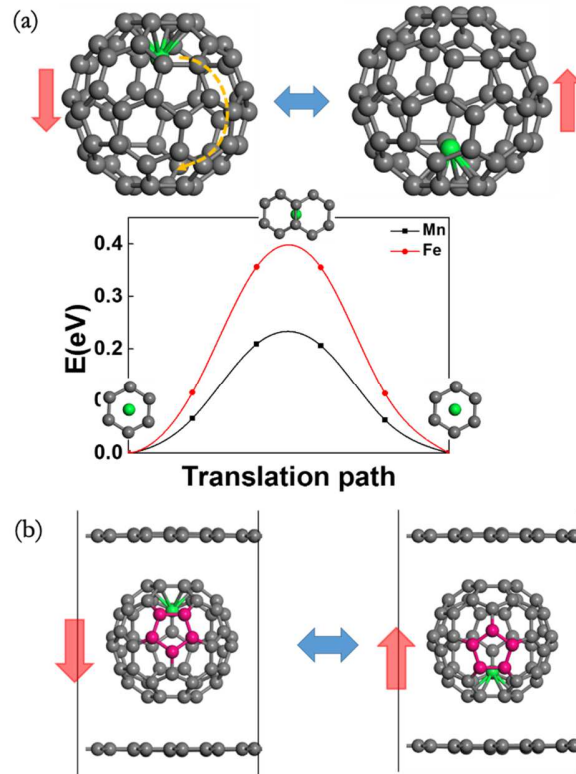


Figure 10. Ferroelectric switching pathway of (a) isolated $M@C_{60}$ fixed on the substrate, and (b) $M@C_{60}$ intercalated between two graphene layers, with a C5 ring in pink to mark the rotation. The polarization directions are denoted by red arrows. Grey and green spheres denote carbon and transition metal atoms, respectively. Adapted with permission from Ref. 60

4.3.2 One-dimensional Nanowires and Two-dimensional functionalized graphene

Ferrocene, $Fe(C_5H_5)_2$, and molecular sandwich nanowire (SNW) are one-dimensional systems. The former is composed of a Fe atom sandwiched between two Cp (C_5H_5) rings while the latter is a one-dimensional chain with formula M_nX_{n+1} where n number of transition metal atoms M are sandwiched between $(n+1)$ Cp or Bz (C_6H_6) rings X^{61-63} . Note that seven-decker $V_7(Bz)_8$ sandwich nanowire has been successfully synthesized in the laboratory. These pristine SNWs are all non-polar. When the H atoms in the Cp or Bz rings are replaced by superhalogen $-OH$, the hydroxyl groups form into hydrogen-bonded chains, resulting in polarization along the SNW

direction. As shown in Fig. 11(a), this polarization can be switched by an applied electric field⁶⁴. For example, in a fully hydroxylized MnCp SNWs 3D crystal where SNWs are connected by hydrogen bonds, a polarization of $23.0 \mu\text{C}/\text{cm}^2$ is obtained. This is larger than the polarization in croconic acid ($21 \mu\text{C}/\text{cm}^2$) at room temperature.

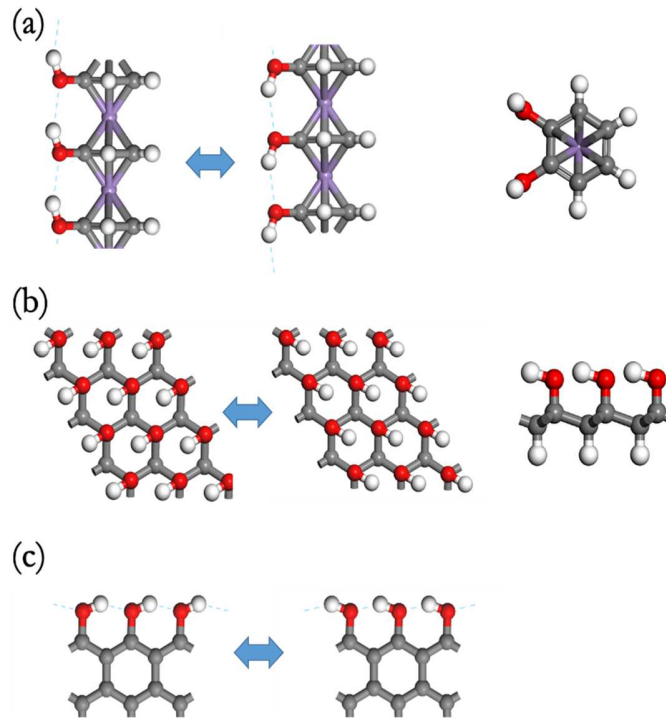


Figure 11. Ferroelectric switching of hydroxylized (a) transition-metal molecular sandwich nanowires, (b) graphene, and (c) graphene nanoribbons (GNR). Grey, red, white, and purple spheres denote C, O, H, and transition metal atoms, respectively. Adapted with permission from Ref. 60

A two-dimensional (2D) van der Waals ferroelectrics can be constructed by functionalizing graphene⁶⁵ with superhalogens. Note that functionalization of graphene results in a non-polar system when all the carbon atoms are saturated with atomic hydrogen/fluorine. However, if the hydrogen/fluorine atoms on one side are substituted by hydroxyl groups, as

shown in Fig.11(b), a 2D hydrogen-bonded network with an in-plane polarization of $41.1\mu\text{C}/\text{cm}^2$ can be formed due to symmetry-breaking by the dipoles of -OH. The polarization can be further increased to $43.7\mu\text{C}/\text{cm}^2$ by replacing the hydrogen atoms in a semi-hydrogenated graphone by -OH groups and stacking these layers on top of each other. The polarization can be switched through the rotation of -OH by an external electric field. One-dimensional ferroelectricity can also be formed when the zigzag-edges of graphene nanoribbons (GNR) are decorated with -OH groups that form hydrogen bonds with adjacent -OH groups, giving rise to a spontaneous polarization. As shown in Fig. 11(c), the displacements of a proton are switchable through the rotation of -OH bond along the direction of GNR.

4.3.3 Three-dimensional Supersalts

Typical salts such as alkali halides are binary systems that crystalize into rock salt (RS) or Cesium Chloride (CsCl) structures. Due to directionless ionic bonding interactions, these structures are all non-polar and centro-symmetric. As mentioned before, materials with mixed ionic-covalent bonding such as BaTiO_3 and PbTiO_3 are well-known perovskite ferroelectrics⁶⁶. Supersalts composed of superalkali cations and superhalogens anions could become polar due to their inherent anisotropy that breaks centro-symmetry. If such breaking can induce switchable polarization, highly ionic ferroelectrics may be formed⁶⁷. Recently, Wu and coworkers⁶⁸ used PH_4 superalkali and BCl_4 superhalogen to construct a supersalt PH_4BCl_4 (Fig. 12(a)). The ground-state structure of PH_4BCl_4 , displayed in Fig. 12(b), is a distorted zinc-blende (dZB) structure that is non-centrosymmetric where both PH_4 and BCl_4 ions retain their pristine forms. The authors carried out an extensive search for similar $\text{NH}_4\text{MX}_4/\text{PH}_4\text{MX}_4$ supersalts ($\text{M}=\text{Al}$ and B and $\text{X}=\text{Cl}$, Br) and found that the ground state structures of these materials have dZB type structure with a slightly different relative angle between the cation tetrahedra and anion

tetrahedra. More importantly, PH_4FeBr_4 is found to possess a dZB ground state structure where magnetism, ferroelectricity, and ferroelasticity are all coupled, making it a long-sought “triferroic” material.⁶⁹

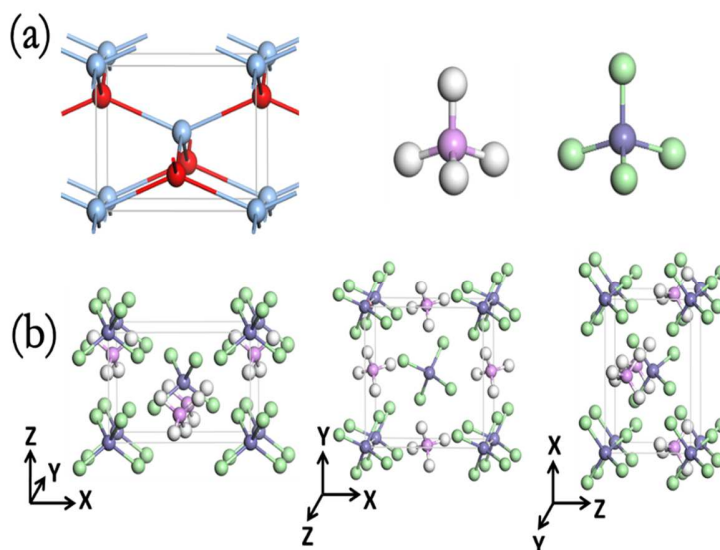


Figure 12. (a) Zinc-blende structure, superalkali cations and superhalogen anions, (b) geometric structures of supersalts $\text{NH}_4\text{MX}_4/\text{PH}_4\text{MX}_4$. Adapted with permission from Ref. 68.

5. Conclusions and Future Outlook

In summary, we have demonstrated that the size and composition of an atomic cluster can be tailored to mimic the chemistry of atoms in the periodic table. These are referred to as superatoms. While the emphasis in this perspective is on superhalogens and superalkalis, clusters can be designed to mimic the chemistry of chalcogens and pnictogens. Because of their large size and aspherical geometry, superatoms have unusual properties. In particular, we highlighted superhalogens that are stable when multiply charged and how these species promote unusual reactions not possible through conventional chemistry. For example, noble gas atom Ar can form chemical bonds with the super-electrophilic species at room temperature, and group 12

metal atom Zn can exhibit an oxidation state of +3. Also discussed is the use of superatoms as building blocks of materials with desired properties. Examples of such cluster-based materials include solar cells, electrolytes in Li-ion batteries, and multiferroic materials. These results offer exciting possibilities where clusters not only can bridge our understanding of how properties evolve one atom at a time but also how their unique size and composition-specific properties can be leveraged to create materials with desired properties.

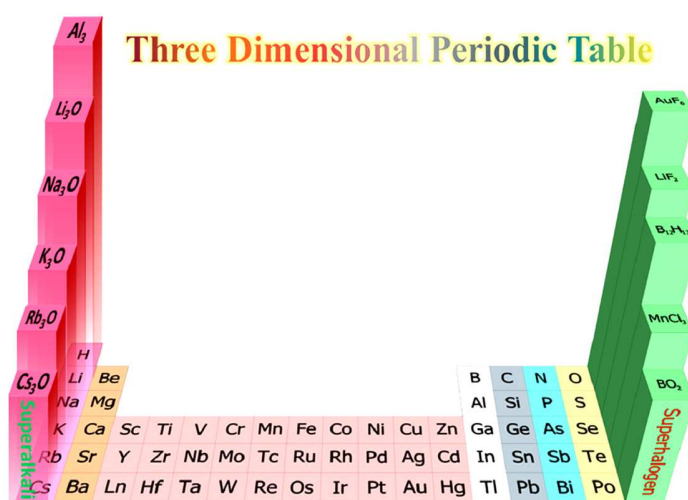


Figure 13. Three-dimensional periodic table with superatoms mimicking the chemistry of halogens and alkalis. Examples are those of superalkalis designed using the octet rule and superhalogens designed using different electron counting rules; Al_{13}^- and Al_{20} (jellium rule), MnCl_3 , and PtF_6 (octet rule), WSi_{12} (18 electron rule), and Al_4H_6 (Wade-Mingos rule). Adapted with permission from ref. 4.

Superatoms can thus be used to create a new three-dimensional periodic table (see Fig. 13) where they form the third dimension. Unlike the conventional periodic table that is limited by the naturally occurring elements, the third dimension of the new periodic table, in principle, will have no such limits. While the future is hard to predict, we may someday realize the alchemists' dream.

Acknowledgments: I thank the Indian Chemical Society for the Prof. A. K. Chandra Memorial Award. This work is partially supported by the U.S. Department of Energy, Office of Basic Energy Sciences, Division of Materials Sciences and Engineering under Award DE-FG02-96ER45579.

References

- 1 S. N. Khanna and P. Jena, Assembling crystals from clusters, *Phys. Rev. Lett.*, 1992, **69**, 1664–1667.
- 2 S. N. Khanna and P. Jena, Atomic clusters: Building blocks for a class of solids, *Phys. Rev. B*, 1995, **51**, 13705–13716.
- 3 G. L. Gutsev and A. I. Boldyrev, DVM- $X\alpha$ calculations on the ionization potentials of MX_{k+1}^- complex anions and the electron affinities of MX_{k+1} “superhalogens”, *Chem. Phys.*, 1981, **56**, 277–283.
- 4 P. Jena and Q. Sun, Super Atomic Clusters: Design Rules and Potential for Building Blocks of Materials, *Chem. Rev.*, 2018, **118**, 5755–5870.
- 5 W. D. Knight, K. Clemenger, W. A. de Heer, W. A. Saunders, M. Y. Chou and M. L. Cohen, Electronic Shell Structure and Abundances of Sodium Clusters, *Phys. Rev. Lett.*, 1984, **52**, 2141–2143.
- 6 R. E. Leuchtner, A. C. Harms and A. W. Castleman, Thermal metal cluster anion reactions: Behavior of aluminum clusters with oxygen, *J. Chem. Phys.*, 1989, **91**, 2753–2754.
- 7 X. Li, H. Wu, X.-B. Wang and L.-S. Wang, *s-p* Hybridization and Electron Shell

- Structures in Aluminum Clusters: A Photoelectron Spectroscopy Study, *Phys. Rev. Lett.*, 1998, **81**, 1909–1912.
- 8 B. K. Rao and P. Jena, Evolution of the electronic structure and properties of neutral and charged aluminum clusters: A comprehensive analysis, *J. Chem. Phys.*, 1999, **111**, 1890–1904.
- 9 W.-J. Zheng, O. C. Thomas, T. P. Lippa, S.-J. Xu and K. H. Bowen, The ionic KAl_{13} molecule: A stepping stone to cluster-assembled materials, *J. Chem. Phys.*, 2006, **124**, 144304.
- 10 X.-B. Wang, C.-F. Ding, L.-S. Wang, A. I. Boldyrev and J. Simons, First experimental photoelectron spectra of superhalogens and their theoretical interpretations, *J. Chem. Phys.*, 1999, **110**, 4763–4771.
- 11 G. L. Gutsev, B. K. Rao and P. Jena, Photodecomposition of MnO_4^- : A Theoretical Study, *J. Phys. Chem. A*, 1999, **103**, 10819–10824.
- 12 X. Li, B. Kiran, J. Li, H.-J. Zhai and L.-S. Wang, Experimental observation and confirmation of icosahedral $W@Au_{12}$ and $Mo@Au_{12}$ molecules., *Angew. Chem. Int. Ed. Engl.*, 2002, **41**, 4786–4789.
- 13 P. Pyykkö and N. Runeberg, Icosahedral WAu_{12} : a predicted closed-shell species, stabilized by aurophilic attraction and relativity and in accord with the 18-electron rule., *Angew. Chem. Int. Ed. Engl.*, 2002, **41**, 2174–2176.
- 14 B. Z. Child, S. Giri, S. Gronert and P. Jena, Aromatic Superhalogens, *Chem. – A Eur. J.*, 2014, **20**, 4736–4745.

- 15 B. Pathak, D. Samanta, R. Ahuja and P. Jena, Borane derivatives: a new class of super- and hyperhalogens., *Chemphyschem*, 2011, **12**, 2423–2428.
- 16 M. Yadav, H. Fang, S. Giri and P. Jena, Ligand stabilization of manganocene dianions – in defiance of the 18-electron rule, *Phys. Chem. Chem. Phys.*, 2019, **21**, 24300–24307.
- 17 M. Willis, M. Götz, A. K. Kandalam, G. F. Ganteför and P. Jena, Hyperhalogens: Discovery of a New Class of Highly Electronegative Species, *Angew. Chemie Int. Ed.*, 2010, **49**, 8966–8970.
- 18 K. Wade, The structural significance of the number of skeletal bonding electron-pairs in carboranes the higher boranes and borane anions and various transition-metal carbonyl cluster compounds, *J. Chem. Soc. D*, 1971, 792–793.
- 19 D. M. P. MINGOS, A General Theory for Cluster and Ring Compounds of the Main Group and Transition Elements, *Nat. Phys. Sci.*, 1972, **236**, 99–102.
- 20 K. Wade, Structural and Bonding Patterns in Cluster Chemistry, *Adv. Inorg. Chem. Radiochem.*, 1976, **18**, 1–66.
- 21 D. M. P. Mingos, Polyhedral skeletal electron pair approach, *Acc. Chem. Res.*, 1984, **17**, 311–319.
- 22 H. Zhao, J. Zhou and P. Jena, Stability of B₁₂(CN)₁₂²⁻: Implications for Lithium and Magnesium Ion Batteries, *Angew. Chemie Int. Ed.*, 2016, **55**, 3704–3708.
- 23 M. Mayer, V. van Lessen, M. Rohdenburg, G.-L. Hou, Z. Yang, R. M. Exner, E. Aprà, V. A. Azov, S. Grabowsky, S. S. Xantheas, K. R. Asmis, X.-B. Wang, C. Jenne and J. Warneke, Rational design of an argon-binding superelectrophilic anion, *Proc. Natl. Acad.*

- Sci.*, 2019, **116**, 8167–8172.
- 24 M. M. Zhong, H. Fang, Deepika and P. Jena, Super-electrophiles of tri- and tetra-anions stabilized by selected terminal groups and their role in binding noble gas atoms, *Phys. Chem. Chem. Phys.*, 2021, **23**, 21496–21500.
- 25 H. Fang, D. Deepika and P. Jena, Binding of noble gas atoms by superhalogens, *J. Chem. Phys.*, 2021, **155**, 14304.
- 26 M. M. Zhong, H. Fang and P. Jena, Record-high stability and compactness of multiply-charged clusters aided by selected terminal groups, *Phys. Chem. Chem. Phys.*, 2020, **22**, 4880–4883.
- 27 H. Fang and P. Jena, Stable Tetra- and Penta-Anions in the Gas Phase, *Angew. Chemie - Int. Ed.*, 2019, **58**, 11248–11252.
- 28 L. Pauling, The Formulas of Antimonic Acid and the Antimonates, *J. Am. Chem. Soc.*, 1933, **55**, 1895–1900.
- 29 N. Bartlett, Xenon Hexafluoroplatinate(v) $\text{Xe} + [\text{PtF}_6]^-$, *Proc. Chem. Soc.*, 1962, 218.
- 30 W. Grochala, Atypical compounds of gases, which have been called ‘Noble’, *Chem. Soc. Rev.*, 2007, **36**, 1632–1655.
- 31 K. O. Christe, A Renaissance in Noble Gas Chemistry., *Angew. Chem. Int. Ed. Engl.*, 2001, **40**, 1419–1421.
- 32 L. Khriachtchev, M. Räsänen and R. B. Gerber, Noble-Gas Hydrides: New Chemistry at Low Temperatures, *Acc. Chem. Res.*, 2009, **42**, 183–191.
- 33 L. Khriachtchev, M. Pettersson, N. Runeberg, J. Lundell and M. Räsänen, A stable argon

- compound, *Nature*, 2000, **406**, 874–876.
- 34 D. Samanta, Prediction of Superhalogen-Stabilized Noble Gas Compounds, *J. Phys. Chem. Lett.*, 2014, **5**, 3151–3156.
- 35 R. L. Deming, A. L. Allred, A. R. Dahl, A. W. Herlinger and M. O. Kestner, Tripositive mercury. Low temperature electrochemical oxidation of 1,4,8,11-tetraazacyclotetradecanemercury(II) tetrafluoroborate, *J. Am. Chem. Soc.*, 1976, **98**, 4132–4137.
- 36 M. Kaupp and H. G. von Schnering, Gaseous Mercury(IV) Fluoride, HgF₄: An Ab Initio Study, *Angew. Chemie*, 1993, **32**, 861–863.
- 37 M. Kaupp, M. Dolg, H. Stoll and H. G. von Schnering, Oxidation state +IV in group 12 chemistry. Ab initio study of zinc(IV), cadmium(IV), and mercury(IV) fluorides, *Inorg. Chem.*, 1994, **33**, 2122–2131.
- 38 X. Wang, L. Andrews, S. Riedel, and M. Kaupp, Mercury is a transition metal: the first experimental evidence for HgF₍₄₎., *Angew. Chem. Int. Ed. Engl.*, 2007, **46**, 8371–8375.
- 39 S. Riedel, M. Kaupp and P. Pyykkö, Quantum Chemical Study of Trivalent Group 12 Fluorides, *Inorg. Chem.*, 2008, **47**, 3379–3383.
- 40 D. Samanta and P. Jena, Zn in the +III Oxidation State, *J. Am. Chem. Soc.*, 2012, **134**, 8400–8403.
- 41 H. Fang, H. Banjade, Deepika and P. Jena, Realization of the Zn³⁺ oxidation state, *Nanoscale*, 2021, **13**, 14041–14048.
- 42 S. Giri, S. Behera and P. Jena, Superhalogens as building blocks of halogen-free

- electrolytes in lithium-ion batteries., *Angew. Chem. Int. Ed. Engl.*, 2014, **53**, 13916–13919.
- 43 O. Tutusaus, R. Mohtadi, T. S. Arthur, F. Mizuno, E. G. Nelson and Y. V. Sevryugina, An Efficient Halogen-Free Electrolyte for Use in Rechargeable Magnesium Batteries., *Angew. Chem. Int. Ed. Engl.*, 2015, **54**, 7900–7904.
- 44 W. S. Tang, A. Unemoto, W. Zhou, V. Stavila, M. Matsuo, H. Wu, S. Orimo and T. J. Udovic, Unparalleled lithium and sodium superionic conduction in solid electrolytes with large monovalent cage-like anions, *Energy Environ. Sci.*, 2015, **8**, 3637–3645.
- 45 J. Zheng, B. Perry and Y. Wu, Antiperovskite Superionic Conductors: A Critical Review, *ACS Mater. Au*, 2021, **1**, 92–106.
- 46 H. Fang and P. Jena, Li-rich antiperovskite superionic conductors based on cluster ions, *Proc. Natl. Acad. Sci. U. S. A.*, 2017, **114**, 11046–11051.
- 47 G. Hodes, Perovskite-Based Solar Cells, *Science*, 2013, **342**, 317-318.
- 48 C. Eames, J. M. Frost, P. R. F. Barnes, B. C. O'Regan, A. Walsh and M. S. Islam, Ionic transport in hybrid lead iodide perovskite solar cells, *Nat. Commun.*, 2015, **6**, 7497.
- 49 H. Fang and P. Jena, Super-ion inspired colorful hybrid perovskite solar cells, *J. Mater. Chem. A*, 2016, **4**, 4728–4737.
- 50 P. Schouwink, M. B. Ley, A. Tissot, H. Hagemann, T. R. Jensen, Ľ. Smrčok and R. Černý, Structure and properties of complex hydride perovskite materials, *Nat. Commun.*, 2014, **5**, 5706.
- 51 H. W. Kroto, J. R. Heath, S. C. O'Brien, R. F. Curl and R. E. Smalley, C60:

- Buckminsterfullerene, *Nature*, 1985, **318**, 162–163.
- 52 J. R. Heath, S. C. O'Brien, Q. Zhang, Y. Liu, R. F. Curl, F. K. Tittel and R. E. Smalley, Lanthanum complexes of spheroidal carbon shells, *J. Am. Chem. Soc.*, 1985, **107**, 7779–7780.
- 53 S. Aoyagi, E. Nishibori, H. Sawa, K. Sugimoto, M. Takata, Y. Miyata, R. Kitaura, H. Shinohara, H. Okada, T. Sakai, Y. Ono, K. Kawachi, K. Yokoo, S. Ono, K. Omote, Y. Kasama, S. Ishikawa, T. Komuro and H. Tobita, A layered ionic crystal of polar Li@C₆₀ superatoms, *Nat. Chem.*, 2010, **2**, 678–683.
- 54 H. J. Chandler, M. Stefanou, E. E. B. Campbell and R. Schaub, Li@C₆₀ as a multi-state molecular switch., *Nat. Commun.*, 2019, **10**, 2283.
- 55 T. Ogawa, T. Sugai and H. Shinohara, Isolation and Characterization of Er@C₆₀, *J. Am. Chem. Soc.*, 2000, **122**, 3538–3539.
- 56 T. Kanbara, Y. Kubozono, Y. Takabayashi, S. Fujiki, S. Iida, Y. Haruyama, S. Kashino, S. Emura and T. Akasaka, Evidence for endohedral structure and electron transfer, *Phys. Rev. B*, 2001, **64**, 113403.
- 57 Y. Kubozono, T. Ohta, T. Hayashibara, H. Maeda, H. Ishida, S. Kashino, K. Oshima, H. Yamazaki, S. Ukita and T. Sogabe, Preparation and Extraction of Ca@C₆₀, *Chem. Lett.*, 1995, **24**, 457–458.
- 58 Y. Kubozono, H. Maeda, Y. Takabayashi, K. Hiraoka, T. Nakai, S. Kashino, S. Emura, S. Ukita and T. Sogabe, Extractions of Y@C₆₀, Ba@C₆₀, La@C₆₀, Ce@C₆₀, Pr@C₆₀, Nd@C₆₀, and Gd@C₆₀ with Aniline, *J. Am. Chem. Soc.*, 1996, **118**, 6998–6999.

- 59 Q. Yang, T. Zhong, Z. Tu, L. Zhu, M. Wu and X. C. Zeng, Design of Single-Molecule Multiferroics for Efficient Ultrahigh-Density Nonvolatile Memories., *Adv. Sci. (Weinh)*, 2019, **6**, 1801572.
- 60 Wu, M.; Jena, P. Superatom-based Ferroelectrics in Superatoms Jena, P. and Sun, Q., Editors, "Superatoms: Principles, Synthesis, and Applications", Wiley (in press)
- 61 L. Hedberg and K. Hedberg, Molecular Structure of Dicyclopentadienylnickel (C₅H₅)₂Ni, *J. Chem. Phys.*, 1970, **53**, 1228–1234.
- 62 E. Gard, A. Haaland, D. P. Novak and R. Seip, The molecular structures of dicyclopentadienylvanadium, (C₅H₅)₂V, and dicyclopentadienylchromium, (C₅H₅)₂Cr, determined by gas phase electron diffraction, *J. Organomet. Chem.*, 1975, **88**, 181–189.
- 63 A. Almenningen, E. Gard, A. Haaland and J. Brunvoll, Dynamic Jahn–Teller effect and average structure of dicyclopentadienylcobalt, (C₅H₅)₂Co, studied by gas phase electron diffraction, *J. Organomet. Chem.*, 1976, **107**, 273–279.
- 64 M. Wu, J. D. Burton, E. Y. Tsymbal, X. C. Zeng and P. Jena, Multiferroic Materials Based on Organic Transition-Metal Molecular Nanowires, *J. Am. Chem. Soc.*, 2012, **134**, 14423–14429.
- 65 M. Wu, J. D. Burton, E. Y. Tsymbal, X. C. Zeng and P. Jena, Hydroxyl-decorated graphene systems as candidates for organic metal-free ferroelectrics, multiferroics, and high-performance proton battery cathode materials, *Phys. Rev. B*, 2013, **87**, 81406.
- 66 R. E. Cohen, Origin of ferroelectricity in perovskite oxides, *Nature*, 1992, **358**, 136–138.
- 67 L. Li, M. Wu and Z. Cheng, Facile and Versatile Functionalization of Two-Dimensional

Carbon Nitrides by Design: Magnetism/Multiferroicity, Valleytronics, and Photovoltaics, *Adv. Funct. Mater.*, 2019, **29**, 1905752.

68 Y. Gao, M. Wu and P. Jena, A family of ionic supersalts with covalent-like directionality and unconventional multiferroicity, *Nat. Commun.*, 2021, **12**, 1331.

69 P. Wadley, B. Howells, J. Železný, C. Andrews, V. Hills, R. P. Campion, V. Novák, K. Olejník, F. Maccherozzi, S. S. Dhesi, S. Y. Martin, T. Wagner, J. Wunderlich, F. Freimuth, Y. Mokrousov, J. Kuneš, J. S. Chauhan, M. J. Grzybowski, A. W. Rushforth, K. W. Edmonds, B. L. Gallagher and T. Jungwirth, Electrical switching of an antiferromagnet, *Science*, 2016, **351**, 587–590.

